A Journal of the Gesellschaft Deutscher Chemiker

Angewandte International Edition Chemie

GDCh

www.angewandte.org

Accepted Article

Title: Rational Design of Specific Recognition Molecules for Simultaneously Monitoring of Endogenous Polysulfide and Hydrogen Sulfide in the Mouse Brain.

Authors: Hui Dong, Qi Zhou, Limin Zhang, and Yang Tian

This manuscript has been accepted after peer review and appears as an Accepted Article online prior to editing, proofing, and formal publication of the final Version of Record (VoR). This work is currently citable by using the Digital Object Identifier (DOI) given below. The VoR will be published online in Early View as soon as possible and may be different to this Accepted Article as a result of editing. Readers should obtain the VoR from the journal website shown below when it is published to ensure accuracy of information. The authors are responsible for the content of this Accepted Article.

To be cited as: *Angew. Chem. Int. Ed.* 10.1002/anie.201907210
Angew. Chem. 10.1002/ange.201907210

Link to VoR: http://dx.doi.org/10.1002/anie.201907210
http://dx.doi.org/10.1002/ange.201907210

WILEY-VCH

10.1002/anie.201907210

WILEY-VCH

Rational Design of Specific Recognition Molecules for Simultaneously Monitoring of Endogenous Polysulfide and Hydrogen Sulfide in the Mouse Brain

Hui Dong, Qi Zhou, Limin Zhang, and Yang Tian**

Abstract: *The correlation and distinction between H_2S_n and H_2S playing in brain function remain the subject of considerable debate. Herein, an efficient biosensor was created for the simultaneous monitoring of endogenous H_2S_n and H_2S in mouse brains and exploring their roles in activation of the TRPA1 channel under two types of brain disease models-ischemia and Alzheimer's disease (AD). Integrated with density functional theory (DFT) calculation and electrochemical measurements, the novel probes, 3,4-bis((2-fluoro-5-nitrobenzoyl)oxy)-benzoic acid (M_{PS-1}) and N-(4-(2,5-dinitrophenoxy) phenyl)-5-(1, 2-dithiolan-3-yl)pentanamide (M_{HS-1}) were rationally designed and synthesized for specific recognition of H_2S_n and H_2S. Through co-assembly of the two probes at the mesoporous gold film (mAu) with good anti-biofouling ability and high electrocatalytic activity, this single microsensor showed high selectivity for H_2S_n and H_2S against potential biological interferences including sulfur-containing species. The present biosensor can simultaneously determine the concentration of H_2S_n from 0.2 to 50 μM, as well as that of H_2S from 0.2 to 40 μM. Finally, using this useful tool, the expression of TRPA1 protein was found to be positively correlated with the levels of H_2S_n under both ischemia and AD.*

The correlation and distinction between hydrogen sulfide (H_2S), and its potential oxidized forms, hydrogen polysulfide (H_2S_n, n>1), in physiological and pathological processes in the brain remain the subject of considerable debate.[1] In the past decades, H_2S has been extensively studied as a signalling molecule.[2] However, recent investigation has revealed that H_2S_n might act as the real regulators in cell signalling transduction. Some biological activities initially attributed to H_2S were hypothesized to be mediated by H_2S_n.[3] An important example is protein S-sulfhydration, which has proven to be a major signalling pathway involving sulfur. From a chemical reactivity point-of-view, H_2S cannot simply "persulfidate" a thiol group. By contrast, H_2S_n possesses stronger oxidation ability than H_2S. Thus, H_2S_n should be more active in S-sulfydration than H_2S.[4] A few studies have given the support that H_2S_n is the actual signalling molecule in protein S-sulfhydration.[4] Unfortunately, the lack of efficient strategies for simultaneous detection of H_2S_n and H_2S in the brain has been a bottleneck to better understanding of the pathophysiological roles of H_2S_n and H_2S.

To date, only a few fluorescent probes have been reported for the determination of H_2S_n.[4a, 5] However, to the best of our knowledge, no efficient approach has been reported for in vivo determination of H_2S_n. In vivo electrochemical analysis of chemical signals in the brain using implanted microsensors is a vital way to study brain function due to high temporal and spatial resolutions.[6] But H_2S_n is electrochemically inert, and generates a Faradic signal beyond the potential window of water splitting. This characteristic leads to great difficulty in direct determination of H_2S_n in aqueous solution, depending on the Faradic signal of H_2S_n. On the other hand, H_2S in principle can be oxidized at the working electrode with the transfer of two electrons ($H_2S \rightarrow S+2H^++2e^-$, $E_{S/H2S}$ at 0.144 V (vs NHE, pH 7.4) at a high overpotential. As a result, the detection of H_2S often suffers from great interferences of other electroactive species in the central nervous system.[7] Although H_2S could be electrochemically oxidized at special metal electrodes such as Ni, V_2O_5 at low potentials, the electrochemical reaction generally occurs in acid (pH <2) or basic media (pH >12).[7] Recently, Zhang et al. developed an electrochemical sensor for in vivo monitoring of H_2S at a low potential of -0.19 V (vs. Ag/AgCl) in the brain by applying ammineruthenium (III) to catalyze the electrochemical oxidation of H_2S in a neutral solution.[8] However, a key issue about electrode contamination should be carefully considered based on the electrochemical oxidation of H_2S because the oxidation product of H_2S, sulfur (S), is strongly adsorbed onto the electrode surface to poison the electrode, resulting in low reproducibility and big determination error. Therefore, it still renders a great challenge to design an efficient sensing strategy to simultaneous assay of H_2S_n and H_2S without cross-talk and electrode contamination.

Motivated by the above challenges, we rationally designed and synthesized the specific recognition molecules for H_2S_n and H_2S, 3,4-bis((2-fluoro-5-nitrobenzoyl)oxy)-benzoic acid (M_{PS-1}) and N-(4-(2,5-dinitro-phenoxy) phenyl)-5-(1,2-dithiolan-3-yl) pentanamide (M_{HS-1}) (Scheme 1) by integrating density functional theory (DFT) calculation with electrochemical measurements. Through co-assembly of M_{PS-1} and M_{HS-1} molecules at the microelectrode decorated by mesoporous gold film (mAu), we successfully evaluated the levels of H_2S_n and H_2S in

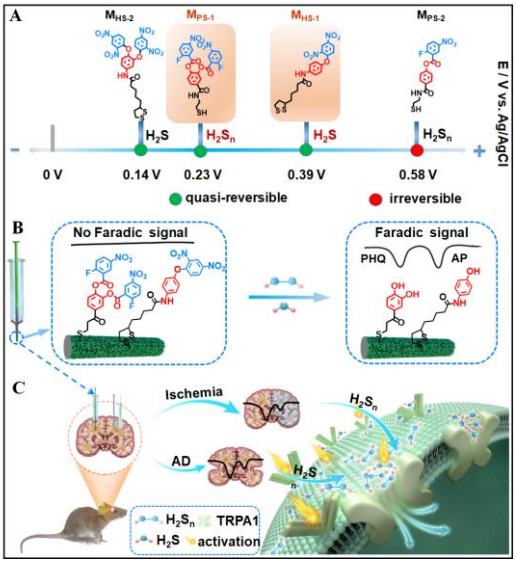

Scheme 1. (A) Probes designed in the proposed sensing strategy. (B) Working principle of M_{PS-1} and M_{HS-2} for specific recognition of H_2S and H_2S_n. (C) Simultaneous assaying of H_2S and H_2S_n in a live mouse brain and further investigation of the activation of the TRPA1 channel by H_2S_n and H_2S.

[*] Hui Dong, Qi Zhou, Prof. Limin Zhang, Prof. Yang Tian
Shanghai Key Laboratory of Green Chemistry and Chemical Processes, School of Chemistry and Molecular Engineering, East China Normal University, Dongchuan Road 500, Shanghai 200241 (China)
E-mail: ytian@chem.ecnu.edu.cn; lmzhang@chem.ecnu.edu.cn
Supporting Information for this article is given via a link at the end of the document.

Accepted Manuscript

This article is protected by copyright. All rights reserved.

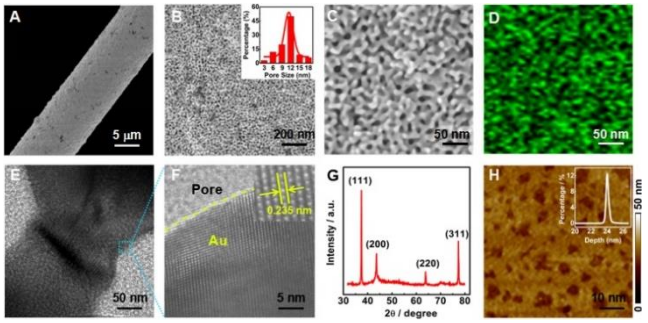

Figure 1. (A) SEM image of CFME coated by mAu. (B-C) Top-surface images, (D) X-ray spectroscopy analysis, (E-F) High-resolution TEM images, (G) XRD pattern, and (H) Atomic force microscopy (AFM) image of the mAu.

the mouse brains with ischemia and AD, and further explored the relationship between the activation of transient receptor potential ankyrin 1 (TRPA1) channel and levels of H_2S_n and H_2S.

As a starting point for this work, mAu was in-situ synthesized at carbon fibre microelectrode (CFME) (Figure 1A).[9] Mesopores with averaged diameter of 11 ± 7 nm were distributed in the entire area (Figure 1B-1D). Moreover, several crystal domains were connected continuously to create a concave surface, which exposed the high index plane (Figure 1E). The lattice spacing of 0.235 nm was attributed to the Au (111) plane of fcc crystal, suggesting the formation of crystalline Au at CFME (Figure 1F-1G) with an averaged pore depth of 24 ± 1 nm, as indicated by AFM (Figure 1H).

H_2S_n is a combination of polysulfide species. The dissolution of any polysulfide salts results in a similar distribution of these species. H_2S_2 is a typical active species of H_2S_n, and remains in dynamic equilibrium with other H_2S_n.[10] Thus, H_2S_2 was taken as a representative target for H_2S_n detection. The compound containing bis-electrophilic groups was envisoned to selectively capture H_2S_2. One of the electrophilic groups was designed to be a latent electroactive group and was released under nucleophilic reaction. Based on this strategy, M_{PS-1} and 4-((2-fluoro-5-nitrobenzoyl)oxy)benzoic acid (M_{PS-2}) were designed (Scheme 1A). They underwent nucleophilic cyclization to form benzodithiolone products after reacted with H_2S_2, resulting in electroactive pyrocatechol (PHQ) released from M_{PS-1}, as well as phenol (PN) from M_{PS-2} (Figure 2E-2F). Additionally, M_{HS-1} and N-(3,4-bis(2,5-dinitrophenoxy)-phenyl)-5-(1,2-dithiolan-3-yl)pentanamide (M_{HS-2}), were designed for recognition of H_2S based on the mechanism in which thiolysis of the dinitrophenyl ether reaction was chemoselective for H_2S.[11] A -NH group was devised at the 4'-site of the phenol derivatives to increase the electron cloudy density of the aromatic ring to tune the response signal for H_2S at a relatively low potential. Once M_{HS-1} and M_{HS-2} reacted with H_2S, nucleophilic substitution occurred, and 5-(1,2-dithiolan-3-yl)-N-(4-hydroxy phenyl) pentanamide (AP) and N-(3,4-dihydroxyphenyl)-5-(1,2-dithiolan-3-yl) pentanamide (NP) were released from M_{HS-1} and M_{HS-2}, respectively. The DFT calculation was performed to rationalize the design of the electrochemical probes. For the oxidation of PHQ, the prevailing mechanism consisting of a $2e^-$-$2H^+$ process was considered. The higher HOMO energy of PHQ than its oxidized state represented a typical characteristic of redox couples (Figure 2A). In contrast, the oxidation process of PN was deduced to be irreversible because the PN radical cation generated by PN spontaneously convert to PHQ due to the small HOMO-LUMO energy gap (0.6 eV) (Figure 2B, 2F). For the specific probes for H_2S, the chemical products, AP and NP, possessed higher HOMO and LOMO energies than their oxidized states, which suggested that they were redox characteristics. With comparison of the Gibbs free energy (ΔG^0) and oxidation potential (E^0), M_{HS-1} and M_{PS-1} were optimized for simultaneous detection of H_2S_n and H_2S because the Faradic signals of PHQ (E^0 = 0.16 V) and AP (E^0 = 0.32 V) were well separated (Supporting Information, Table S1).

This design concept was then confirmed by a series of experiments. All the probes were synthesized and characterized (Figure S1-S4). The sensing strategy was based on the typical proceeding chemical reactions. FTIR spectroscopy and LC-MS were used to confirm the chemical products of four probes with targets. Combined with the peak at ~3273 cm^{-1} (-OH group), new m/z peaks of 154.03 and 138.03 confirmed that the chemical products of M_{PS-1} and M_{PS-2} with H_2S_n were PHQ and PN (Figure S5-S7), respectively. Similarly, the products of M_{HS-1} and M_{HS-2} with H_2S, AP and NP, were confirmed by the m/z peaks of 298.09 and 336.07 (Figure S8-S9). According to the results, the chemical reactions of four probes were summarized (Scheme S2), and the corresponding equilibrium constants (k) were estimated (Figure S10). The four designed probes showed similar k values, which provided a similar response time during simultaneous determination.

The electrochemical behaviors of all the probes were investigated by cyclic voltammetry (CV). M_{PS-1} and M_{PS-2} were assembled at cysteamine (Cyst)-decorated CFME/mAu to form CFME/mAu/M_{PS-1} and CFME/mAu/M_{PS-2}, respectively. Meanwhile, M_{HS-1} and M_{HS-2} were modified at CFME/Au to fabricate CFME/Au/M_{HS-1} and CFME/Au/M_{HS-2}, respectively. Each modification step was recorded by CV and XPS (Figure S11). No obvious peak was obtained at CFME/mAu and CFME/mAu/M_{PS-1} in blank aCSF. However, a pair of redox peaks with a half-wave potential ($E_{1/2}$) of ~ 0.25 ± 0.03 V were observed at CFME/mAu/M_{PS-1} in aCSF containing 30 μM Na_2S_2 (Figure 2I). This peak was ascribed to the redox process of the formed PHQ moiety at CFME/mAu/M_{PS-1}. In comparison, only one irreversible anodic peak with E_P of 0.61 V was obtained at CFME/-mAu/M_{PS-2} due to the oxidation of PN (Figure 2J). However, this peak rapidly decreased to the basal level during the second cycle of scanning. This unstable Faradic response was hard to apply in the brain. On the other hand, a couple of redox peaks with good stability were both observed at CFME/mAu/M_{HS-1} and CFME/mAu/M_{HS-2} after the addition of 30 μM H_2S, which were attributed to the redox processes of AP ($E_{1/2}$ = 0.35 V) and NP moieties ($E_{1/2}$ = 0.08 V) (Figure 2K, 2L). The heterogeneous electron transfer constants (k_s) of four generated electroactive probes at electrodes were estimated by using the Laviron method (Figure S12, and Table S2). Larger k_s values of PHQ (5.06 ± 0.12 s^{-1}) and AP (4.91 ± 0.17 s^{-1}) indicate their faster kinetic processes than those of PN (0.52 ± 0.30 s^{-1}) and NP (4.17 ± 0.09 s^{-1}). Accordingly, it was rational to select M_{PS-1} and M_{HS-1} as the probes to construct a single sensor for simultaneous detection of H_2S_n and H_2S because of well-separated Faradic signals, good stability, and fast electrochemical kinetic processes.

Subsequently, Cyst and M_{HS-1} were co-assembled at CFME/mAu to form CFME/mAu/Cyst+M_{HS-1}. M_{PS-1} was further confined to result in CFME/mAu/M_{PS-1}+M_{HS-1}. The surface coverages of M_{PS-1} and M_{HS-1} were estimated to be 31.8 pmol cm^{-2} for M_{PS-1}, 21.6 pmol cm^{-2} for M_{HS-1}. Each modification step was characterized by differential pulse voltammetry (DPV) because of its high sensitivity (Figure S13). No Faradic current was observed at CFME/mAu, CFME/mAu/Cyst+M_{PS-1}, and CFME/mAu/M_{PS-1}+M_{HS-1} in blank aCSF (Curves a-c). Only one cathodic peak, with E_p values of 0.21 V and 0.39 V, were observed at

Accepted Manuscript

This article is protected by copyright. All rights reserved.

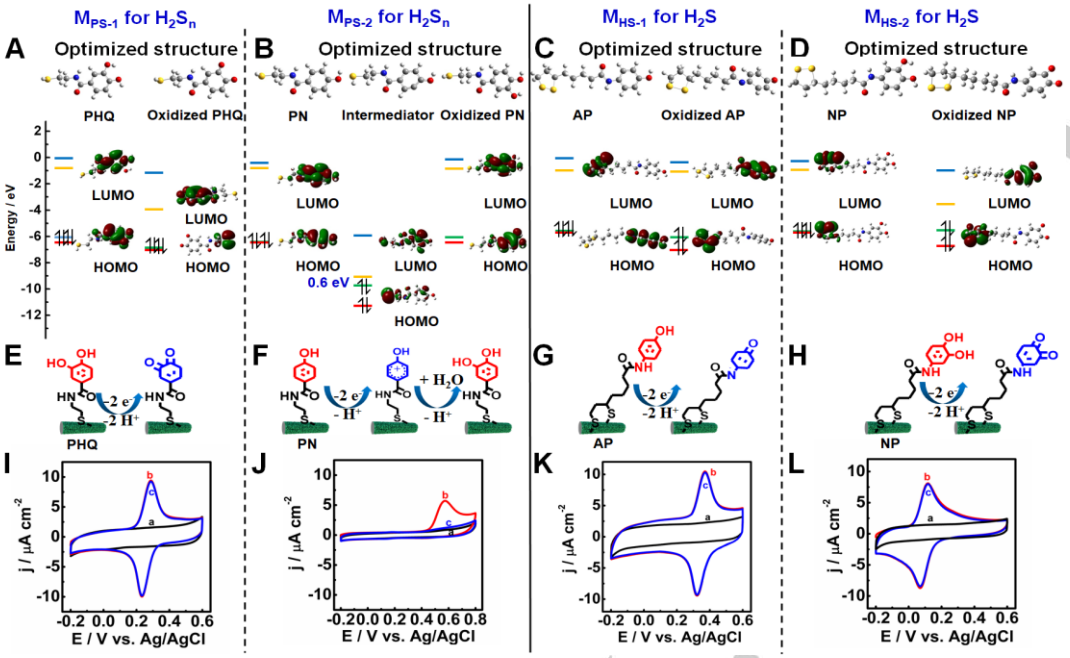

Figure 2. Optimized ground-state geometries of PHQ (A), PN (B), AP (C) and NP (D) in its oxidized and reduced forms calculated using DFT methods. From top to bottom, images correspond to top view, side view, molecular orbital energy level, and HOMO and LUMO shapes. Electrochemical reactions (E-H) and CVs obtained at (I) CFME/mAu/M_{PS-1}, (J) CFME/mAu/M_{PS-2} in aCSF (pH 7.4) in the absence (a) and presence of 30 μM Na_2S_2 before (b) and after (c) scanning for 100 cycles, and CVs obtained at (K) CFME/mAu/M_{HS-1}, (L) CFME/mAu/M_{HS-2} in the absence (a) and presence of 30 μM Na_2S before (a) and after (b) 100 cycles of scanning. Scan rate: 100 mV s^{-1}.

CFME/mAu/M_{PS-1}+M_{HS-1} after the addition of 30 μM Na_2S_2 and 30 μM Na_2S, respectively. These peaks were ascribed to the reduction of PHQ and AP (Curve f and g). As expected, two well-separated cathodic peaks were obtained at 0.22 V and 0.39 V after the simultaneous addition of 30 μM Na_2S_2 and 30 μM Na_2S (Curve h). Both of M_{PS-1} and M_{HS-1} exhibited fast responses for Na_2S_2 and Na_2S within 40 s (Figure S14). On the one hand, j_p value at 0.21 V (denoted as $j_{p(PHQ)}$) gradually increased with an increasing concentration of Na_2S_2, exhibiting a good linearity from 0.2 to 60 μM (Figure 3A, 3A'), while j_p value at 0.39 V ($j_{p(AP)}$) kept almost constant. On the other hand, $j_{p(AP)}$ showed a good linearity with the concentration of Na_2S ranging from 0.2 to 50 μM in the presence of 30 μM Na_2S_2 (Figure 3B, B'). During simultaneous measurements, negligible cross-talk was observed between the responsive channels of Na_2S_2 and Na_2S. When the concentrations of Na_2S_2 and Na_2S were simultaneously increased, good linearities were obtained between $j_{p(PHQ)}$ with the concentration of Na_2S_2 from 0.2 to 50 μM, as well as between $j_{p(AP)}$ and the concentration of Na_2S from 0.2 to 40 μM (Figure 3C, 3C'). The detection limits were estimated to be 40 ± 3 nM for H_2S_n, and 47 ± 4 nM for H_2S. Derived from the high roughness of mAu, $j_{p(PHQ)}$ and $j_{p(AP)}$ at CFME/mAu/M_{PS-1}+M_{HS-1} was 5.1-fold greater than obtained at the gold electrode modified with M_{PS-1} and M_{HS-1} (Au/M_{PS-1}+M_{HS-1}) (Figure S15). Moreover, the developed biosensor exhibited high selectivity. Interferences smaller than 4.0% and 5.1% were observed for $j_{p(PHQ)}$ and $j_{p(AP)}$ upon the addition of potential interferences, particularly sulfur-containing species (Figure S16), even though several interferences had relatively high concentrations much larger than those of H_2S_n and H_2S. Besides, the negligible current fluctuation as pH shifting from 6.0 to 8.0 suggested the pH stability of measurement signal (Figure S17). Similar measurements for detection of Na_2S_4 using M_{PS-1} probe were also examined (Figure S18), indicating that M_{PS-1} was available for determination of other polysulfides.

The anti-biofouling ability of the present biosensor modified with mAu was examined. Obvious adsorption of BSA was observed at Au/M_{PS-1}+M_{HS-1}, but only weak fluorescence was obtained at CFME/mAu/M_{PS-1}+M_{HS-1} (Figure S19). Additionally, j_p/j_p^0 values (j_p^0 is the initial current density, and j_p is the current density at different time) of PHQ and AP obtained at Au/M_{PS-1}+M_{HS-1} greatly decreased by ~54.0% and 52.7%, but negligible decrease (< 9.2%) was observed at CFME/mAu/M_{PS-1}+M_{HS-1} (Figure S20). To further clarify the roles of the anti-fouling ability of mAu, $Fe(CN)_6^{3-}$ and $Ru(NH_3)_6^{3+}$ with opposite charges, which are sufficiently small to transfer into the mesopores of mAu, were used to estimate the non-specific adsorption of BSA. As expected, the redox peaks of two probes obviously decreased at Au/M_{PS-1}+M_{HS-1} in BSA solution, but changed slightly at CFME/mAu/M_{PS-1}+M_{HS-1} (Figure S21). The results revealed that the adsorption of large biomolecules was restricted by the mesopores of mAu, instead of electrostatic interaction.

The developed biosensor with high selectivity and sensitivity, as well as good anti-fouling ability provided a reliable platform for assaying H_2S_n and H_2S in the brain. Two brain disease models were used: middle cerebral artery occlusion (MCAO) and AD. Figure 4A shows DPVs obtained at CFME/mAu/M_{PS-1}+M_{HS-1} electrode in the hippocampus of a normal mouse brain before and after MCAO. Two cathodic peaks at 0.22 V and 0.39 V were clearly observed (Figure 4A). The standard deviation of $j_{p(PHQ)}$ and $j_{p(AP)}$ for five biosensors tested in the same mouse brain did not exceed 4.8% for H_2S_n and 5.3% for H_2S, indicating good reproducibility of the present biosensor (Figure S22). With the ischemia duration prolonged, the infarction area was gradually increased in the right cerebral hemisphere, indicating the successful mouse MCAO model (Figure 4B). Correspondingly, the concentration of H_2S_n remarkably increased by 336.1%, 376.5%, and 400.3% in the hippocampus, cortex, and striatum of normal mouse brain upon MCAO for 2.0 h, respectively (Figure 4C, Figure S23). To

Accepted Manuscript

This article is protected by copyright. All rights reserved.

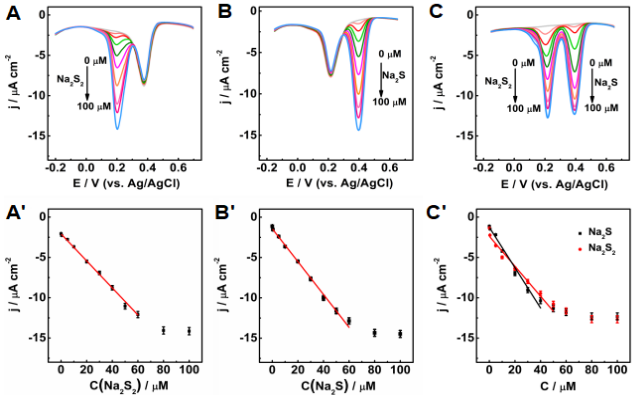

Figure 3. (A) DPVs obtained at the CFME/mAu/M_{PS-1}+M_{HS-1} in aCSF (pH 7.4) containing 30 μM Na_2S and varied Na_2S_2 concentrations from 0.2 to 100 μM. (B) DPVs obtained at the CFME/mAu/M_{PS-1}+M_{HS-1} in aCSF (pH 7.4) containing 30 μM Na_2S_2 and varied Na_2S concentrations ranging from 0.2 to 100 μM. (C) DPVs obtained at the CFME/mAu/M_{PS-1}+M_{HS-1} in aCSF solution (pH 7.4) with simultaneously varied Na_2S_2 and Na_2S concentrations ranging from 0.2 to 100 μM, and (A'-C') Calibration plots of *j* versus Na_2S_2 and Na_2S concentrations obtained from A-C. The error bars indicate standard deviations (n=3, S.D.).

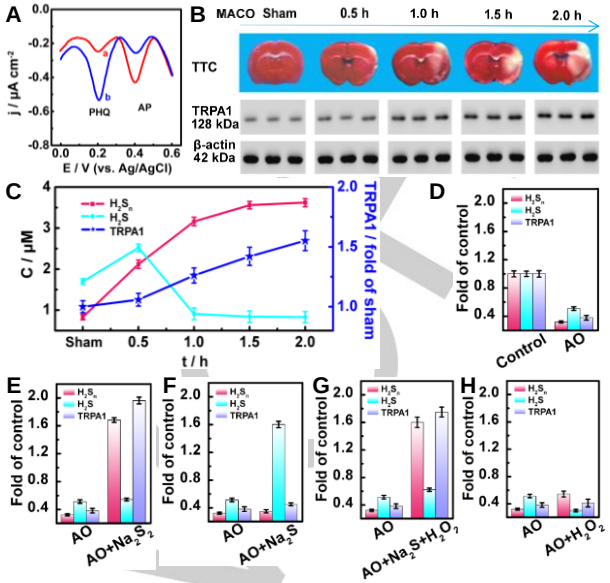

Figure 4. (A) Typical DPVs obtained at CFME/mAu/M_{PS-1}+M_{HS-1} in a mouse brain before (a) and after (b) MCAO for 2.0 h. (B) TTC -staining of ischemic brain slices upon MCAO for different times, and Western blot analysis of the level of TRPA1 protein and β-actin. (C) The levels of H_2S_n, H_2S, and TRPA1 protein in hippocampus upon MACO with different hours. (D) Fold of control for H_2S_n, H_2S, and TRPA1 expression obtained in mouse brain slices after AO treatment, (E) and successive stimulation by Na_2S_2, (F) Na_2S, (G) Na_2S and H_2O_2, and (H) H_2O_2. The concentrations of Na_2S_2, Na_2S and H_2O_2 in experiments were 10 μM. The Error bars indicate standard deviations (n=3, S.D.).

our surprise, the concentration of H_2S first increased in the initial 0.5 h MCAO, but fell down in the following 1.5 h MCAO. This observation was completely different from previous report.[12] The initial increase of H_2S was possibly due to the remarkedly elevated level of cysteine.[13] However, H_2S was gradually consumed by the produced ROS, resulting in the decrease in the level of H_2S with the ischemia duration prolonged. After reperfusion, both of the peak currents returned to nearly basal levels (Figure S24). Similar measurements were conducted to track the variation of H_2S_n and H_2S in the mouse brain with AD. Compared with those in the normal brain, the levels of H_2S_n increased to 2.65 ± 0.33 μM, 2.77 ± 0.31 μM, and 2.81± 0.24 μM in the hippocampus, cortex, and striatum of APP/PS1 Tg mice, and the H_2S levels decreased to 0.98± 0.17 μM, 0.68 ± 0.16 μM, and 0.69 ± 0.13 μM (Table S3).

Recent investigation has revealed that TRPA1 channel, a Ca^{2+} permeable channel, plays important roles in ischemia and AD.[14] Meanwhile, H_2S and H_2S_n are two potential molecules to activate TRPA1 channel via S- sulfhydration. Therefore, it is meaningful to explore the relationship between TRPA1 channel, and H_2S_n and H_2S in the brain with ischemia and AD. Western blot analysis was first used to track the expression of TRPA1 proteins in the mouse brain slices. Compared with that of the normal brain, the level of TRPA1 protein upregulate by 5.0% to 55.3% as MCAO time increased from 0.5 h to 2.0 h (Figure 4C). Interestingly, different from H_2S, the variation of TRPA1 protein exhibited positive correlation with the level of H_2S_n in the mouse brain under ischemia (Figure 4C). In addition, similar positive correlation between TRPA1 protein and the concentration of H_2S_n was observed in brain slices from wild mice and APP/PS1 Tg mice (Figure S25-S26).[4c] Previous studies have mainly focused on the activity of H_2S on S -sulfhydration of protein,[15] even if H_2S_n has been reported to be generated through oxidation of H_2S, and shows high oxidation ability.[1b,16] Our observation suggested that H_2S_n was possibly the actual molecule to activate TRPA1 channel.

To further verify the roles of H_2S and H_2S_n in the activation of TRPA1 channel, our useful tool was extended to monitor the levels of H_2S_n and H_2S in the hippocampal mouse brain slices under different stimulation. Cysteine is the main substance to generate H_2S.[17] Through exogenous addition of 10 μM amino-oxyacetate (AO) (the inhibitor of cysteine), the generation of H_2S was efficiently blocked by reducing the amount of cysteine (Figure 4D). As expected, the amounts of H_2S and H_2S_n in the brain slice were apparently decreased by 49.0% and 68.0%, and the TRPA1 protein downregulated by 62.1% (Figure 4D). As demonstrated above, the levels of H_2S and H_2S_n in the brain slices were significantly decreased after the slices were treated by AO, which were considered as basal conditions. Then, the treated brain slices were exogenously stimulated by Na_2S_2 (10 μM). The level of H_2S_n dramatically increased to 425.0%, but the level of H_2S slightly increased by 5.9% (Figure 4E). Meanwhile, a remarkable increase in TRPA1 protein of 415.8% was observed. By contrast, in the treated brain slices stimulated by Na_2S (10 μM), the level of H_2S increased apparently, while negligible variation was obtained for both of H_2S_n and TRPA1 protein (Figure 4F). The results suggested that H_2S failed to generate H_2S_n and to elevate the protein expression of TRPA1 channel, possibly due to lack of sufficient oxidant.[1c] Thus, followed by the experiments above, we next stimulated the brain slices by H_2O_2 after addition of H_2S, because H_2O_2 has been previously reported to facilitate the endogenous generation of H_2S_n from H_2S.[4c] As expected, the amount of H_2S was gradually reduced with increasing concentration of H_2O_2, but remarkable enhancement of H_2S_n amount was observed (Figure 4G). Meanwhile, it was noteworthy that the protein expression of TRPA1 channels was increased with increasing amount of H_2S_n upon H_2O_2 stimulation (Figure S27). However, for the control experiment, negligible changes were obtained for TRPA1 protein upon stimulation by only H_2O_2 using the slices treatment by AO (Figure 4H) without addition of H_2S and H_2S_2, demonstrating that H_2O_2 cannot activate TRPA1 channel. Thus, the activation of TRPA1 channel were more positively correlated with H_2S_n, which was consistent with our results observed in the brain under ischemia and AD (Figure 4C, Figure S26). These findings provided an evidence that

Accepted Manuscript

This article is protected by copyright. All rights reserved.

H_2S_n might a more efficient molecule for activation of TRPA1 channel than H_2S.

In summary, using DFT calculation and electrochemical measurements, we have rationally designed and synthesized M_{PS-1} and M_{HS-1} as specific probes for the chemical recognition of H_2S_n and H_2S, respectively. Based on M_{PS-1} and M_{HS-1}, a single electrochemical biosensor was created to simultaneously determine H_2S_n and H_2S levels in vivo in the mouse brains with MCAO and AD. In addition, mAu synthesized at CFME can improve the sensitivity, and presents good anti-biofouling capability. This biosensor not only showed high selectivity for H_2S_n and H_2S against potential interferences in the brain, but was also able to avoid electrode contamination from sulfur absorption. Using this in vivo biosensor, we observed the variation of H_2S_n and H_2S in mouse brains under ischemia and AD. More interestingly, H_2S_n was found to exhibit a stronger ability to activate TRPA1 channel than H_2S. This investigation gives impetus to reacquaintance of the molecular mechanism of H_2S and H_2S_n. More importantly, this study also supplies an approach for designing single biosensors for the determination of multiple species closely related to physiological and pathological events in the brain.

Acknowledgements. **S**upport by National Natural Science Foundation of China (Nos. 21635003, 21827814 for Y. T. and 21675054 for L. Z.), Innovation Program of Shanghai Municipal Education Commission (201701070005E00020).

Keyword: Brain chemistry • Biosensors • Analytical Methods • Polysulfide • Hydrogen sulfide

[1] a) T. V. Mishanina, M. Libiad, R. Banerjee, *Nat. Chem. Bio.* **2015,** *11*, 457; b) H. Kimura, *Proc. Jpn. Acad. Ser. B* **2015,** *91*, 131; c) R. Greiner, Z. Palinkas, K. Basell, D. Becher, H. Antelmann, P. Napy, T. P. Dick, *Antioxid. Redox Signaling* **2013,** *19*, 1749.

[2] a) M. Eberhardt, M. Dux, B. Namer, J. Miljkovic, N. Cordasic, C. Will, T. I. Kichko, J. de la Roche, M. Fischer, S. A. Suarez, D. Bikiel, K. Dorsch, A. Leffler, A. Babes, A. Lampert, J. K. Lennerz, J. Jacobi, M. A. Marti, F. Doctorovich, E. D. Hogestatt, P. M. Zygmunt, I. Ivanovic-Burmazovic, K. Messlinger, P. Reeh, M. R. Filipovic, *Nat. Commun.* **2014,** *5*, 4381; b) E. Blackstone, M. Morrison, M. B. Roth, *Science* **2005,** *308*, 518; c) C. Szabo, *Nat. Rev. Drug Discovery* **2007,** *6*, 917.

[3] a) P. K. Yadav, M. Martinov, V. Vitvitsky, J. Seravalli, R. Wedmann, M. R. Filipovic, R. Banerjee, *J. Am. Chem. Soc.* **2016,** *138*, 289; b) B. Tan, P. T.-H. Wong, J. S. Bian, *Neurochem. Int.* **2010,** *56*, 3; c) J. W. Elrod, J. W. Calvert, J. Morrison, J. E. Doeller, D. W. Kraus, L. Tao, X. Jiao, R. Scalia, L. Kiss, C. Szabo, H. Kimura, C. W. Chow, D. J. Lefer, *Pro. Natl. Acad. Sci. U. S. A.* **2007,** *104*, 15560.

[4] a) B. Yu, Y. Zheng, Z. Yuan, S. Li, H. Zhu, L. K. De La Cruz, B. Wang, *J. Am. Chem. Soc.* **2018,** *140*, 30; b) Y. Kimura, Y. Mikami, K. Osumi, M. Tsugane, J. Oka, H. Kimura, *FASEB J.* **2013,** *27*, 2451.

[5] a) C. Liu, W. Chen, W. Shi, B. Peng, Y. Zhao, H. Ma, M. Xian, *J. Am. Chem. Soc.* **2014**, *136*, 7257; b) V. S. Lin, W. Chen, M. Xian, C. J. Chang, *Chem. Soc. Rev.* **2015,** *44*, 4596.

[6] a) A. G. Ewing, J. C. Bigelow, R. M. Wightman, *Science* **1983,** *221*, 169; b) G. S. Wilson, M. C. Johnson, *Chem. Rev.* **2008,** *108*, 2462; c) D. L. Robinson, A. Hermans, A. T. Seipel, R. M. Wightman, *Chem. Rev.* **2008,** *108*, 2554; d) W. Liu, H. Dong, L. Zhang, Y. Tian, *Angew. Chem. Int. Ed.* **2017,** *56*, 16328; e) L. Liu, F. Zhao, W. Liu, T. Zhu, J. Zhang, C. Chen, Z. Dai, H. Peng, J. Huang, Q. Hu, W. Bu, Y. Tian, *Angew. Chem. Int. Ed.* **2017,** *56*, 10471; f) Y. Luo, L. Zhang, W. Liu, Y. Yu, Y. Tian, *Angew. Chem. Int. Ed.* **2015,** *54*, 14053; g) X. Chai, X. Zhou, A. Zhu, L. Zhang, Y. Qin, G, Shi, Y. Tian, *Angew. Chem. Int. Ed.* **2013,** *52*, 8129; h) L. Zhang, Y. Tian, *Acc. Chem. Res.* **2018,** *51*, 688; i) J. Zhou, L. Zhang, Y. Tian, *Anal. Chem.* **2016,** *88*, 2113; j) L. Zhang, F. Liu, X. Sun, G. Wei, Y. Tian, Z. Liu, R. Huang, Y. Yu, H. Peng, *Anal. Chem.* **2017,** *89*, 1831.

[7] a) D. Giovanelli, N. S. Lawrence, L. Jiang, T. G. J. Jones, R. G. Compton, *Sens. Actuators B* **2003,** *88*, 320; b) J. A. Bennett, J. E. Pander, M. A. Neiswonger, *J. Electroanal. Chem.* **2011,** *654*, 1.

[8] S. Wang, X. Liu, M. Zhang, *Anal. Chem.* **2017,** *89*, 5382.

[9] C. Li, O. Dag, T. Dao, T. Nagao, Y. Sakamoto, T. Kimura, O. Terasaki, Y. Yamauchi, *Nat. Commun.* **2015,** *6*, 6608.

[10] P. Nagy, Z. Palinkas, A. Nagy, B. Budai, I. Toth, A. Vasas, *Biochim. Biophys. Acta* **2014,** *1840*, 876.

[11] C. Liu, B. Peng, S. Li, C. Park, A. R. Whorton, M. Xian, *Org. Lett.* **2012,** *14*, 2184.

[12] a) K. Qu, C. P. Chen, B. Halliwell, P. K. Moore, P. T-H. Wong, *Stroke* **2006,** *37*, 889; b) Z. Li, Y. Wang, Y. Xie, Z. Yang, T. Zhang, *Neurochem. Res.* **2011,** *36*, 1840.

[13] a) K. Abe, H. Kimura, *J. Neurosci.* **1996,** *16*, 1066; b) C. Ren, A. Du, D. Li, J. Sui, W. Mayhan, H. Zhao, *Brain Res.* **2010,** *1345*, 197.

[14] a) K. Lee, H. Lee, H. Lin, H. Tsay, F. Tsai, S. Shyue, T. Lee, *J. Neuroinflammation.* **2016,** *13*, 92; b) P. W. Pires, S. Earley, *Elife* **2018,** *7*, e35316.

[15] A. K. Mustafa, M. M. Gadalla, N. Sen, S. Kim, W. Mu, S. K. Gazi, R. K. Barrow, G. Yang, R. Wang, S. H. Snyder, *Sci. Signal.* **2009,** *2*, ra72.

[16] Y. Kimura, Y. Mikami, K. Osumi, M. Tsugane, J. Oka, H. Kimura, *FASEB J.* **2013,** *27*, 2452.

[17] R. d'Emmanuele di Villa Bianca, R. Sorrentino, P. Maffia, V. Mirone, C. Imbimbo, F. Fusco, R. De Palma, L. J. Ignarro, G. Cirino, *Proc. Natl. Acad. Sci.* **2009,** *106*, 451.

Accepted Manuscript

WILEY-VCH

This article is protected by copyright. All rights reserved.

10.1002/anie.201907210

WILEY-VCH

The correlation and distinction between H_2S_n and H_2S playing in brain function remain the subject of considerable debate. A novel single electrochemcial sensor was created for simultaneous detection of H_2S_n and H_2S in brain. With our sensor, the expression of TRPA1 channel was found to be positively correlated with the levels of H_2S_n in two brain disease models under ischemia and Alzheimer's diseases, and H_2S_n is more acitive for expression of TRPA1 protein than that of H_2S.

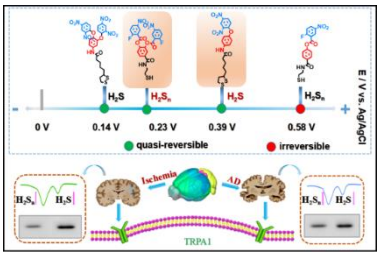

Hui Dong, Qi Zhou, Limin Zhang,* Yang Tian*

Rational Design of Specific Recognition Molecules for Simultaneously Monitoring of Endogenous Polysulfide and Hydrogen Sulfide in the Mouse Brain

WILEY-VCH

Accepted Manuscript

This article is protected by copyright. All rights reserved.